Received: 10 June 2018 | Accepted: 28 August 2018

DOI: 10.1002/jcp.27438

ORIGINAL RESEARCH ARTICLE

WILEY Journal of Cellular Physiology

Potential of bacterial culture media in biofabrication of metal nanoparticles and the therapeutic potential of the as-synthesized nanoparticles in conjunction with artemisinin against MDA-MB-231 breast cancer cells

Badrealam Farheen Khan[1] | Hamidullah[2] | Sonam Dwivedi[2] | Riyuraj Konwar[2*] | Swaleha Zubair[3*] | Mohammad Owais[1*]

[1]Molecular Immunology Laboratory, Interdisciplinary Biotechnology Unit, Aligarh Muslim University, Aligarh, India

[2]Division of Endocrinology, CSIR-Central Drug Research Institute, Lucknow, India

[3]Women's College, Aligarh Muslim University, Aligarh, India

Correspondence
Mohammad Owais, Molecular Immunology Laboratory, Interdisciplinary Biotechnology Unit, Aligarh Muslim University, Aligarh 202002, India.
Email: owais_lakhnawi@yahoo.com
Riyuraj Konwar, Division of Endocrinology, CSIR-Central Drug Research Institute, 10/1 Jankipuram Extension, Lucknow 226031, India.
Email: r_konwar@cdri.res.in
Swaleha Zubair, Women's College, Aligarh Muslim University, Aligarh, Uttar Pradesh 202002, India.
Email: swalehazubair@yahoo.com

Abstract

In the recent past, various groups have proposed diverse biocompatible methods for the synthesis of metal nanoparticles (NPs). Besides culture biomass, culture supernatants (CS) are increasingly being explored for the synthesis of NPs; however, with the ever-increasing exploration of various CS in the biofabrication of NPs, it is equally important to explore the potential of various culture media (CMs) in the synthesis of metal NPs. Considering these aspects, in the present investigation, we explore the possible applicability of various CMs in the biofabrication of metal NPs. The synthesis of NPs was primarily followed by UV/VIS spectroscopy, and, thereafter, the NPs were characterized by various physiochemical techniques, including EM, EDX, FT_IR, X-ray diffraction, and DLS measurements, and finally, their anticancer potentialities were investigated against breast cancer. In addition, the NPs were examined in conjunction with artemisinin for therapeutic benefits against aggressive and highly metastatic MDA-MB-231 breast cancer cells. Cumulatively, the results of the present study collated the potentials of various bacterial CMs in the biofabrication of metal NPs and ascertained the efficacy of the as-synthesized silver nanoparticles, especially the combinatorial entity as intriguing breast cancer therapeutics. The data of the present study plausibly assist in advancing the therapeutic applicability of the combinatorial amalgam against aggressive and highly metastatic MDA-MB-231 breast cancer cells.

KEYWORDS

artemisinin (ART), breast cancer, culture media (CMs), culture supernatants (CS), nanoparticles (NPs)

1 | INTRODUCTION

Over the years, nanobiotechnology has been envisioned as a burgeoning field with immense scope and application in various allied disciplines of science. Among nanosized particles, metal nanoparticles (NPs), especially silver nanoparticles (AgNPs), have lately garnered much attention owing to their various intriguing attributes (Xie, Lee, Wang, & Ting, 2007). Considering their potentials in various technological applications, diverse synthesis methodologies have been and are being explored to meet their ever-increasing demands. Lately, green synthesis methodologies have

*These authors contributed equally to this study.

emerged as eco-friendly and cost-effective alternatives to physical and chemical synthesis methodologies (Shankar et al., 2004; Wei et al., 2015; Xie et al., 2007). Besides, culture biomass, culture supernatants (CS) of various organisms ranging from prokaryotes (microbes) to relatively higher microbes on evolutionary ladder (fungi) to most complex and advanced eukaryotes (plants and animals) have been increasingly explored for the synthesis of metal NPs (Chandran, Chaudhary, Pasricha, Ahmad, & Sastry, 2006; Jo et al., 2016; Kumar & Poornachandra, 2015; Senapati, Ahmad, Khan, Sastry, & Kumar, 2005), benefitting technological application. Although researchers have highlighted the efficacy of various CS for the synthesis of AgNPs, surprisingly, there are inadequate reports ascertaining the plausible role of culture media (CM) in the biofabrication of NPs. To the best of our knowledge, only Shivaji et al. and Yamal et al. have highlighted the role of CM in the biofabrication of AgNPs (Yamal, Sharmila, Rao, & Pardha-Saradhi, 2013; Shivaji, Madhu, & Singh, 2011). however, with the ever-increasing exploration of diverse CS in the biofabrication of NP, it is equally important to explore the potentials of various CMs in the biofabrication of metal NPs. Considering these aspects, in the present investigation, we explore the possible applicability of various CMs in the biofabrication of metal NPs. The synthesis of NPs was primarily followed by UV/VIS spectroscopy, and, thereafter, the particles were characterized by various physiochemical techniques including EM, EDX, X-ray diffraction (XRD), FT_IR, and DLS analysis, which indeed corroborated formation of NPs. Further, these two previous studies were concluded at the phenomenological stage without examining real-world applications of the as-synthesized AgNPs; nevertheless, follow-up studies ascertaining their application in biology and medicine are essentially required as well.

Breast cancer represents an enormous human malignancy worldwide, especially among women (Key, Verkasalo, & Banks, 2001). Despite an active treatment regimen, it is one of the leading causes of death (Key, Verkasalo, & Banks, 2001). In the next set of study, we assessed the potentials of the as-synthesized AgNPs in breast cancer therapeutics. Basically, certain sets of experiments, including cell viability assay, oxidative stress, apoptosis, DNA fragmentation, cell cycle, and western blot analysis, were performed to examine their anticancer efficacy against highly aggressive and metastatic breast cancer. In addition to examining their anticancer potentials individually, we further examined their efficacy in conjunction with artemisinin (ART), a sesquiterpene lactone which is experiencing scrutiny and early trials as promising cancer therapeutic candidate (Krishna, Bustamante, Haynes, & Staines, 2008).

To the best of our knowledge, this is the first report exploring the applicability of various CMs in the biofabrication of diverse metal NPs and ascertaining the efficacy of the as-synthesized AgNPs against breast cancer either alone or in conjunction with ART thereof.

2 | MATERIALS AND METHODS

2.1 | Materials and reagents

All reagents and chemicals were procured from Sigma-Aldrich (St. Louis, MO) unless otherwise mentioned. CMs namely, brain heart infusion (BHI), nutrient broth (NB), and Luria-Bertani (LB) were procured from Hi-Media, Mumbai, India. Tissue CM, reagents, and culture wares were purchased from BD Biosciences, San Diego, CA.

2.2 | Biofabrication of AgNPs

2.2.1 | Biofabrication of AgNPs using various CMs

$AgNO_3$ (0.1 M) solution was incubated with various CMs (BHI, NB, and LB) at room temperature (RT) under continuous stirring condition (120 rpm), and the concomitant reduction of the corresponding ions to the corresponding NPs was ascertained by UV/VIS spectroscopy together with transmission electron microscopy (TEM)/energy dispersive x-ray spectroscopy (EDX) analysis. It should be noted that the concentration of CMs used was same as used for culturing of bacterial species (37 gm/L BHI, 13 gm/L NB, and 25 gm/L LB). Moreover, to ascertain the role of BHI in the biofabrication of other coinage metal NPs namely, gold NPs (AuNPs) and copper NPs (CuNPs); $HAuCl_4$ (0.1 M) and $CuSO_4.5H_2O$ (0.1 M) solutions were incubated with BHI at RT and the concomitant reduction of the corresponding ions was ascertained by UV/VIS spectroscopy and TEM/EDX analysis. Further, to examine the constituents of BHI responsible for the biofabrication of AgNPs, $AgNO_3$ (0.1 M) solution was incubated with various constituents of BHI keeping the molar concentration constant as that in the BHI media (BHI: an admix of calf brain infusion and beef heart infusion, protease peptone, dextrose, sodium chloride, and disodium phosphate) at RT under continuous stirring condition (120 rpm).

2.2.2 | Biofabrication of AgNPs using *Aloe vera* extract

Fresh green *Aloe vera* leaves were obtained from the botanical garden of Aligarh Muslim University with the help of a field botanist. The leaves (30 g) were thoroughly cleaned, finely chopped, and boiled in Milli-Q water to yield 30% *Aloe vera* solution (Chandran et al., 2006). Thereafter, the boiled extract was filtered through a Whatman filter and used for further studies. Basically, $AgNO_3$ (0.1 M) solution was incubated with 30% *Aloe vera* solution at RT under continuous stirring condition (120 rpm), and the reduction of the corresponding ion was followed by UV/VIS spectroscopy together with TEM/EDX analysis.

Following synthesis of NPs, the resultant solutions were pelleted, washed several times with MilliQ H_2O, and finally lyophilized for long-term storage. For subsequent studies, the as-synthesized NPs were resuspended in MilliQ H_2O and sonicated in a bath-type sonicator with intermittent vortexing.

2.3 | Physiochemical characterization of the as-synthesized NPs

2.3.1 | UV/VIS spectroscopy

The corresponding reduction of the Ag ions was examined on a Lambda 25 UV/VIS dual-beam spectrophotometer (PerkinElmer Corp., Waltham, MA) by scanning in the range from 300 to 800 nm with 5 nm resolution. The graphing was done using Sigma Plot

version11 software. The result showed was obtained after slight smoothening of the data using the smooth curve function of the Sigma Plot version11 software package.

2.3.2 | Transmission electron microscopy and energy dispersion X-ray spectroscopy

The as-synthesized NPs were characterized by TEM (JEOL, JEM-2100 transmission electron microscope) for their shape and morphological attributes, whereas the elemental analysis was performed using energy dispersion X-ray spectrometry (EDS, OXFORD INCA) following recommended procedures.

2.3.3 | Scanning electron microscopy and energy dispersion X-ray spectroscopy

The as-synthesized NPs were further characterized by scanning electron microscopy (SEM; JEOL, JSM 6510 LV scanning electron microscope) fitted with Oxford Instruments INCA EDX spectrometer set up for their shape and morphological attributes as well as elemental composition.

2.3.4 | FT_IR spectral analysis

The as-synthesized AgNPs were examined for the presence of various functional groups using an FT_IR spectrum RX-1 instrument (PerkinElmer, Corp., Wellesley, MA). The spectra were recorded between 4000 and 900 cm^{-1} in the diffuse reflectance mode at a resolution of 1 cm^{-1}, using KBr pellets (Oves et al., 2013).

2.3.5 | X-ray diffraction studies

XRD studies were executed to ascertain the crystalline nature of the as-synthesized AgNPs on a Mini-Flex™ II benchtop XRD system (Rigaku Corporation, Tokyo, Japan) in range of $5 \leq 2\theta \leq 85$ operating at a voltage of 40 kV. The graphing was done using PowderX software. The results as-shown are obtained after smoothening the data.

2.3.6 | Dynamic light scattering analysis

The colloidal behavior of the NPs was assessed by determining the hydrodynamic diameter (d_h) and the zeta potential (ζ) with dynamic light scattering (Malvern Zetasizer Nano ZS90 equipped with MPT-2 Autotitrator Malvern Instruments, Malvern, United Kingdom) following the manufacturer's recommended protocol.

2.4 | Anticancerous potential of the as-synthesized AgNPs

2.4.1 | Cell lines

Human breast cancer cell lines (MDA-MB-231 and MCF-7), mouse mammary tumor cell line (4T1), and nonmalignant human embryonic kidney cell line (HEK-293) were cultured in RPMI supplemented with 10% FBS and 1% penicillin–streptomycin solution at 37°C with 5% CO_2 in a humidified chamber. Rat mammary tumor cell line (LA-7) was maintained in DMEM supplemented with 5% FBS, 5 µg/ml insulin, and 50 nM hydrocortisone at 37°C with 5% CO_2 in a humidified chamber.

2.4.2 | Cell viability assay

The cytotoxic potentials of the as-synthesized AgNPs were primarily determined using 3-(4,5-dimethylthiazol-2-yl)-2,5-diphenyltetrazolium bromide (MTT) assay. The cells (1×10^4/well) were seeded in 96-well plates in complete CM for 24 hr. AgNPs were diluted to desired concentrations in CM and incubated with the cells for 24 hr. For the inhibition study, 10 mM N-acetyl-L-cysteine (NAC) was pretreated for 2 hr followed by treatment with AgNPs. For examining their efficacy in conjunction with ART, the cells were treated with 100 µM of ART along with a different concentration of the as-synthesized AgNPs. After a stipulated incubation period of 24 hr, 20 µl of MTT (5 mg/ml) was added to each well followed by further incubation of 3 hr. Thereafter, CM was carefully removed, and 200 µl dimethyl sulphoxide was added to dissolve the formazan crystal and the absorbance was recorded at 540 nm using a microplate reader.

2.4.3 | Colony formation assay

To further ascertain the cytotoxic potentialities of the as-synthesized AgNPs, colony formation assay was carried out in MDA-MB-231 cells. Cells, at a density of 5×10^2/well, were seeded in a six-well plate and allowed to grow for 24 hr. The cells were treated with different concentrations of the as-synthesized AgNPs for 24 hr. After the stipulated incubation period, the cells were washed with PBS and allowed to grow in complete growth media for one week; thereafter, the cells were fixed with ice cold methanol and stained with 1% crystal violet.

2.4.4 | Cell cycle analysis

To evaluate the effect of the as-synthesized AgNPs on cell cycle phase distribution, cell cycle assay was carried out using flow cytometry using propidium iodide (PI) as a probe. Briefly, MDA-MB-231 cells (1×10^6/well) were seeded in six-well plates and allowed to grow for 24 hr. Thereafter, the cells were treated with 2 µg/ml of the as-synthesized AgNPs for 24 hr. At the end of the incubation period, both floating and adherent cells were harvested and fixed with 70% ice cold ethanol at 4°C for 1 hr. Finally, the cells were washed with PBS, resuspended in PBS containing 10 mg/ml RNase A and stained with 30 mg/ml of PI for 30 min at RT in the dark. The DNA content of the cells was measured using a FACS Calibur flow cytometer (Becton Dickinson, San Jose, CA).

2.4.5 | Apoptosis analysis

To determine the effect of the as-synthesized AgNPs on apoptosis, MDA-MB-231 cells (1×10^6) were seeded in six-well plates for 24 hr.

Thereafter, the cells were treated with 2 μg/ml of AgNPs and incubated for 24 hr. In case of ART and NPs, the cells were treated with 100 μM of ART along with 1 μg/ml of as-synthesized AgNPs for 24 hr. At the end of the incubation period, the cells were harvested washed with PBS, resuspended in binding buffer, and stained with annexin V-FITC/PI for 10 min in the dark at RT. Samples were acquired using a FACS Calibur flow cytometer (Becton Dickinson, San Jose, CA).

2.4.6 | Cellular reactive oxygen species (ROS) detection assay

The intracellular reactive oxygen species (ROS) level was determined using 2,7-dichloro dihydro fluorescein diacetate (DCFH-DA) assay after treatment of AgNPs by flow cytometry. MDA-MB-231 cells (1×10^6/well) were seeded in six-well plates for 24 hr. The cells were treated with 2 μg/ml of AgNPs for 24 hr. After the stipulated incubation period, the cells were harvested, washed with PBS, and fixed in ice-cold methanol. Finally, the cells were pelleted, resuspended in PBS, and stained with 30 μg/ml DCFH-DA for 30 min in the dark at RT and acquired using a FACS Calibur flow cytometer (Becton Dickinson, San Jose, CA).

2.4.7 | DNA ladder assay

DNA ladder assay was carried out to determine DNA fragmentation in MDA-MB-231 cells after treatment with the as-synthesized AgNPs. Cells (1×10^6/well) were seeded in six-well plates and allowed to grow for 24 hr. Thereafter, the cells were incubated with 2 μg/ml AgNPs for 24 hr. For the inhibition study, 10 mM NAC was pretreated for 2 hr followed by AgNPs for 24 hr. At the end of the incubation period, the cells were harvested, genomic DNA was isolated using a GenElute mammalian genomic DNA purification kit (Sigma-Aldrich, St. Louis, MO) and resolved by agarose gel electrophoresis.

2.4.8 | Cellular DNA fragmentation ELISA

The DNA fragmentation pattern in MDA-MB-231 cells was further ascertained using a cellular DNA fragmentation ELISA kit as per the manufacturer's instructions (Roche Diagnostics, Mannheim, Germany). Briefly, the cells were labeled with 5-bromo-2-deoxyuridine (BrdU) and, thereafter, incubated with 2 μg/ml of AgNPs for 24 hr. For inhibitor study, 10 mM NAC was pretreated for 2 hr followed by AgNPs for 24 hr. After the stipulated incubation period, the cells were harvested and lysed, and labeled DNA was measured using ELISA with an anti-BrdU antibody.

2.4.9 | Western blot analysis

Alterations in protein expressions profiles in response to AgNPs treatment were examined in MDA-MB-231 cells by using western blotting. MDA-MB-231 cells were treated with 2 μg/ml of AgNPs for 24 hr. After 24 hr, the cells were harvested and lysed in RIPA buffer in the presence of a protease and phosphatase inhibitor cocktail. After quantification with the Bradford method, 40 μg of total protein was resolved by SDS-PAGE. The protein was transferred to a PVDF membrane, blocked with 1% BSA for 1 hr and incubated with primary antibody Bax, Bcl-2, cleaved caspase-3 (cell signaling technology), cleaved PARP (Abcam), Ba processes operative in k and Bcl-xl (Santa Cruz Biotechnology) at 4°C overnight. The blots were then incubated with HRP-conjugated secondary antibody for 2 hr. Signals were developed by using chemiluminescent detection substrate and documented using Image Quant LAS 40 to mediate 10 system significance using m (GE Healthcare Life Sciences, UK). Blots were stripped and reprobed with β-actin (Sigma-Aldrich, St. Louis, MO) mineralization processes operative.

2.5 | Statistical analysis

Data are expressed as mean ± SEM with at least three independent experiments and were subjected to statistical comparison using one-way ANOVA followed by post hoc Newman–Keuls multiple comparison test of significance using GraphPad Prism 3.02 software.

3 | RESULTS AND DISCUSSION

Inspired by the biomineralization processes operative in the biological/natural system, material scientists have unraveled the potentialities of various biofactories to fabricate advanced nanoscale products. Both biomass and CS have been advocated to owe potentials to mediate the synthesis of nanoscale products; interestingly, cell-free CS embodies added advantage in the context of ease of control over the synthesis and purification of the as-synthesized NPs (Gurunathan et al., 2009). Reckoning with these, the research fraternities across the globe progressively delves the potentials of various CS from diverse microbial sources to mediate the synthesis of nanoscale products and various CS are in vogue to be increasingly explored (Jo et al., 2016; Kumar & Poornachandra, 2015; Singh et al., 2015). To this end, with the ever-increasing exploration of diverse CS in biofabrication of NPs, it is equally demanding to ascertain the plausible role of various CMs in biofabrication of NPs. Reckoning with these, in the current study, we explored the applicability of CMs in biofabrication of metal NPs and assessed the potentials of the as-synthesized AgNPs in breast cancer therapeutics either as standalone strategy or in conjunction with ART.

Incubation of $AgNO_3$ solution with LB, BHI, and NB CMs led to the development of opaque whitish, yellowish brown, and dark brownish colored colloidal solution, respectively, which exhibits characteristics SPR bands in the visible region (Figure 1a). No characteristics peaks were observed for neat CMs solution. Further, TEM analysis was performed to decipher the shape and the morphological attributes of the as-synthesized NPs. Interestingly, almost spheroidal shaped AgNPs were evident from TEM analysis (Figure 1bi,iii,v). Moreover, EDX spectroscopy was used to further ascertain the formation of NPs (Figure 1bii,iv,vi). The spectra were

obtained in the spot-profile mode by concentrating the electron beam onto an area having an intense population of NPs. The EDS spectra reveal a major peak approximately at 3 keV, corroborating the absorption of metallic Ag nanocrystals due to their surface plasmon for all the corresponding colloidal solution thus formed upon incubation of $AgNO_3$ with respective CMs (LB, NB, and BHI). Further, we moved ahead to ascertain whether CM could mediate the synthesis of other coinage metals as well including AuNPs and CuNPs. Taking BHI as model media, we set up reaction conditions to foster the generation of NPs (the reason behind selecting BHI to

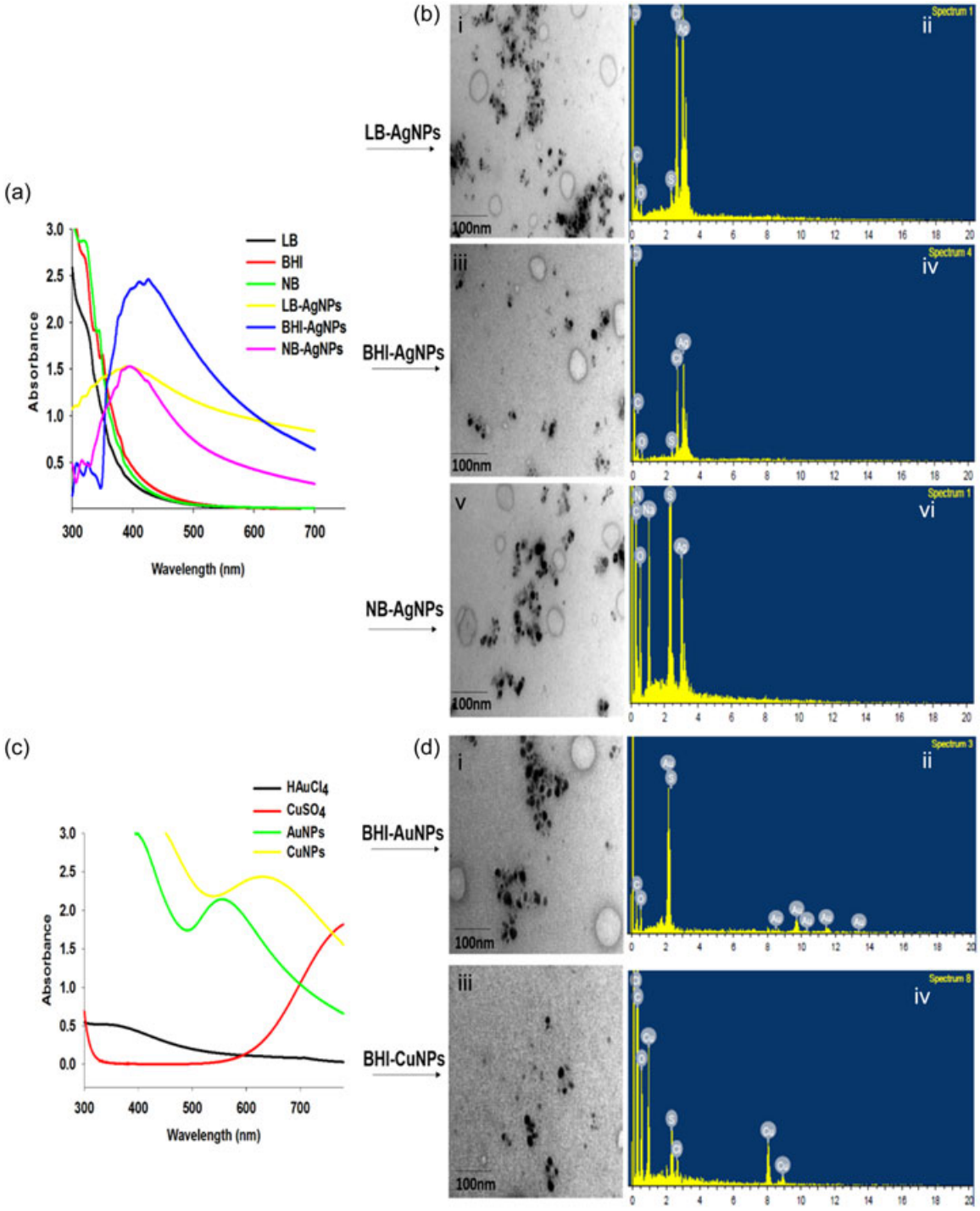

FIGURE 1 Physicochemical characterization of the as-synthesized NPs. (a) Representative UV/VIS spectra of AgNPs following incubation of $AgNO_3$ solution with LB, BHI, and NB CMs, respectivey. (b) Representative TEM micrographs and EDS profile of the as-synthesized AgNPs. (c) Representative UV/VIS spectra of AuNPs and CuNPs following incubation of $HAuCl_4$ and $CuSO_4$ solution with BHI CM. (d) Representative TEM micrographs and EDS profile of the as-synthesized NPs. Spectra of the corresponding neat salt, as well as CMs, are depicted as well. AgNP: silver nanoparticle; AuNP: gold nanoparticle; BHI: brain heart infusion; CM: culture media; CuNP: copper nanoparticle; EDS: energy dispersion X-ray spectrometry; LB: Luria-Bertani; NB: nutrient broth; NP: nanoparticle; TEM: transmission electron microscopy [Color figure can be viewed at wileyonlinelibrary.com]

ascertain formation of metal NPs was that under similar experimental ambiance; compared with other CMs, BHI yielded high yield of NPs as evidenced by higher absorbance intensity). The synthesis was followed by UV/VIS spectroscopy; interestingly but not surprisingly, BHI fostered generation of Au and Cu NPs, as evident by the strong characteristic SPR band in the visible region when analyzed by UV/VIS spectroscopy (Figure 1c), whereas no characteristic SPR bands were observed for the neat salt solutions (Figure 1c) as well as for neat BHI media (Figure 1a). Further, TEM along with EDX analysis was used to further corroborate the formation of NPs. Interestingly, TEM analysis suggested the formation of spheroidal shaped NPs in both the preparations (Figure 1di,iii); whereas the EDS spectra reveals a major peak approximately around 2 keV and in the region of 8–14 keV, corroborating the characteristic X-ray radiation of AuNPs, for the colloidal solution of $HAuCl_4$ and BHI (Figure 1dii); whereas peaks approximately at 0.93 keV and in region around 8 and 9 keV were observed for the colloidal mixtures of BHI and $CuSO_4$, corroborating for the absorption of metallic Cu nanocrystals due to their surface plasmon (Figure 1div). This certainly provides evidence for the formation of corresponding NPs. Further, in the all EDS spectrum, one could certainly observe peak maxima for C, O, and S elements as well besides peaks for the corresponding metals. These peak maxima could be correlated to the molecular entities present in the CMs (Supporting Information Figure S1) which might have played a role in the biofabrication of these NPs and henceforth got coated onto the surfaces of the NPs.

Further, we examined the intricacies underlying generation of AgNPs using BHI; it could be seen that under similar experimental condition using the same molar concentration of BHI constituents; incubation of $AgNO_3$ with BHI constituents (infusions from brain and heart, protease peptone, dextrose, sodium chloride, and disodium phosphate) led to the development of characteristics SPR peak only with infusions from brain and heart, protease peptone and dextrose; whereas no characteristic SPR peak was observed upon incubation with sodium chloride and disodium phosphate which instigate the role of brain heart infusion, protease peptone and dextrose in biofabrication of AgNPs (data not shown). We speculate that the molecular entities especially proteins/carbohydrate (macromolecules comprising of C, N, O, and S) present in the BHI media plausibly play roles in the biofabrication of these NPs; nevertheless, as of yet the exact mechanism advocating biofabrication of NPs remain elusive; further investigations are guaranteed to fully decipher the roles of these molecular entities in the biofabrication of the these NPs.

Evidence supports that microbial assisted synthesis of NPs represents safer and economical alternatives over chemical and physical synthesis methodologies; however, even in these as-synthesized NPs, the chances of contaminants of pathogenic microbes or toxic products cannot be ruled out, which raises concern in their biomedical applicability. To this end, biofabrication of NPs through CMs embodies added advantage of avoiding pathogenic contaminants besides offering sterile NPs as well. Thus, providing nano-therapeutics for plausible prompt biomedical applicability (Yamal et al., 2013).

Finally, we examined their anticancerous potentialities together with AgNPs synthesized with *Aloe vera* extract (Chandran et al., 2006). Moreover, besides ascertaining their efficacy in solitary, we extended further to examine their efficacy in conjunction with ART as well. Basically, ART is a sesquiterpene lactone which has been lately demonstrated to be effective against diverse forms of cancer (Krishna et al., 2008). Albeit, ART enjoys a status of high repute as an effective antimalarial drug; they are in voyage undergoing development as a promising cancer therapeutic candidate. In fact, it has been anticipated as an alternative therapeutic for highly metastatic, aggressive, and drug-resistant tumors (Crespo-Ortiz & Wei, 2012; Xu et al., 2011). As a matter of fact, it is widely accepted that regardless of its potentials, ART suffers from pharmacokinetic limitations; the drug has issues related to its bioavailability and circulatory half-life, which hinder its clinical development.

Before moving ahead, the as-synthesized AgNPs were ascertained for their physiochemical attributes (Figure 2). SEM analysis of the particles purified from the colloidal mixtures reveals the spheriodal morphology of the as-synthesized AgNPs (Figure 2ai and bi), whereas EDS spectra exhibit a strong Ag signal together with feeble C, O, S peaks, basically arising from molecular entities abound to the NPs (Figure 2aii and bii). Further, in the FT_IR analysis of the as-synthesized AgNPs; we could observe distinct peaks approximately around 557cm-1,1046 cm-1, 383cm-1,1624cm-1, and 3416 cm-1 in case of BHI-AgNPs (Fig. 2Ae); whereas broad peaks approximately in region around 580 cm-1 and 34285 cm-1, and distinct peaks around 1406 cm-1, 1530 cm-1, and 1607 cm-1 were evident in Av-AgNPs (Fig. 2Be); besides other minor bands in both the preparations. The band around 557 cm^{-1} represents a characteristic feature of alkynes group of C–H bonds and 1046 cm^{-1} band could be attributed to C–O–H bending vibrations; whereas the band around 1383 cm^{-1} and 1624 cm^{-1} basically originate from carbonyl (C–O) and –NH vibrations in the amide group; moreover, XRD analysis is suggestive of the fact that the as-synthesized AgNPs obeys Braggs model of diffraction. The diffraction peaks concord with the crystalline planes of the face-centered cubic structure of the typical metallic Ag corroborating with the database of Joint Committee on Powder Diffraction Standard (Figure 2aiv and biv) (Oves et al., 2013). Further, the ζ-potential of the as-synthesized AgNPs were in the range of −1.30 and −2.16 mV, respectively for BHI-AgNPs and Av-AgNPs (Figure 2aiii and biii); whereas the hydrodynamic radii (Z-average, d-nm) of the as-prepared BHI-AgNPs and Av-AgNPs were about 262 and 164 nm, respectively (Figure 2avi and bvi).

Further, to explore the potential of the as-synthesized AgNPs against breast cancer, cell viability assay was carried out in human breast cancer cell lines (MDA-MB-231 and MCF-7), rat mammary tumor cell line (LA-7), and mouse mammary tumor cell line (4T1) together with nonmalignant cells (HEK-293). MTT assay, used to assess the effect of AgNPs on the viability of cells, showed a concentration-dependent decrement in formazan product intensity (a marker of cell viability) in all the malignant breast cell lines; signifying that the as-synthesized AgNPs reduced the viability of the cells in a dose-dependent manner (Figure 3a). Whereas no evident reduction in cell viability was observed

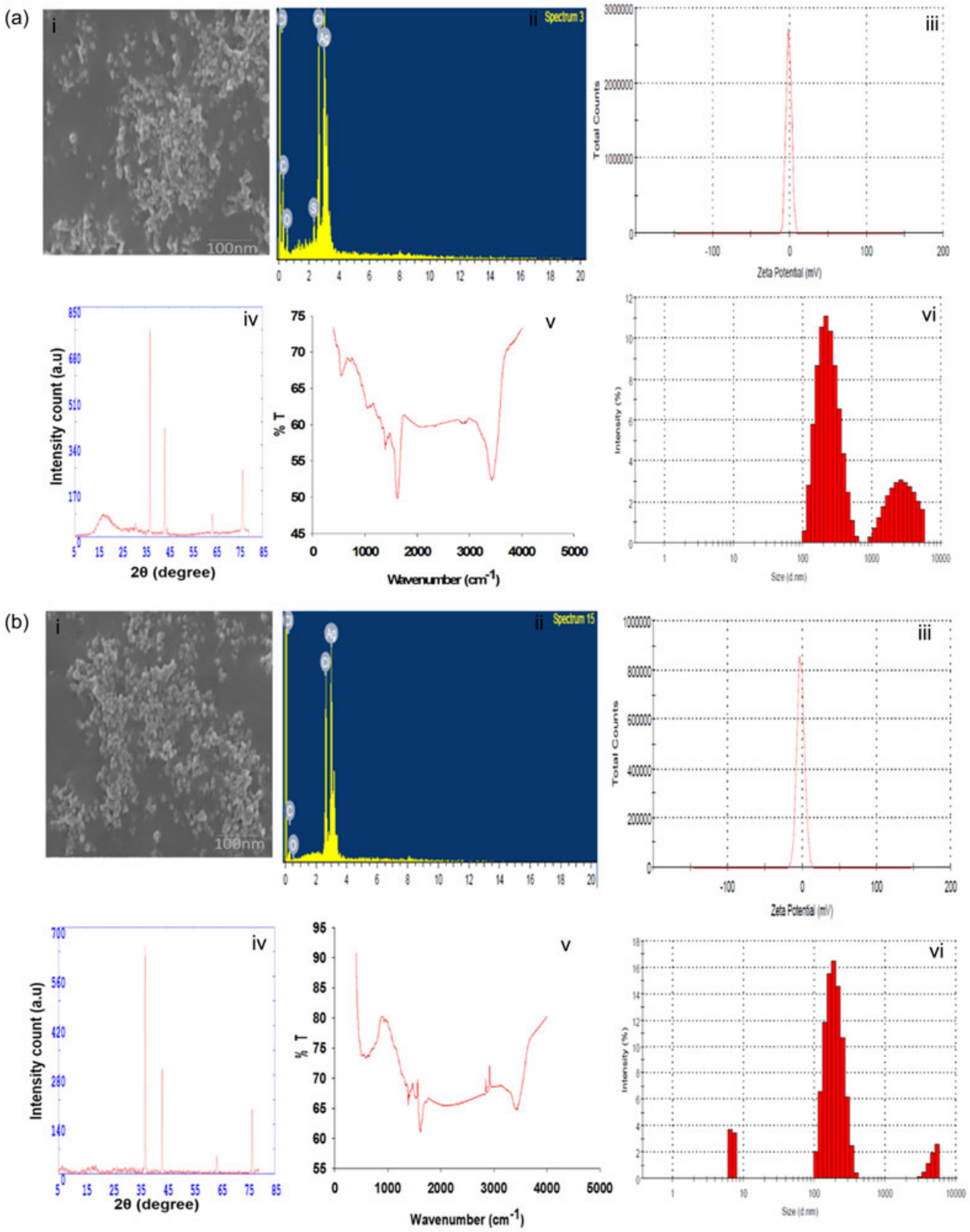

FIGURE 2 Physicochemical characterization of the as-synthesized BHI-AgNPs (a) and Av-AgNPs (b). Representative SEM micrograph (i), EDS profile (ii), zeta potential (iii), XRD pattern (iv), FT_IR spectra (v), and size distribution (vi) of the as-synthesized BHI-AgNPs and Av-AgNPs respectively [Color figure can be viewed at wileyonlinelibrary.com]

for neat BHI and Av extract, these observations endorse biocompatibility of BHI and Av extract and suggest that the cytotoxicity was mainly due to as-synthesized AgNPs. To further ascertain that cytotoxicity mainly arises from the as-synthesized AgNPs and not from any toxic entities left behind after synthesis of NPs, MTT assay was carried out with supernatent obtained after pelleting the NPs, which is supposed to embody excess of such reaction entities (AshaRani, Low Kah Mun, Hande, & Valiyaveettil, 2009); interestingly, we could not observe any apparent reduction in viability of cells treated with the same; data were compared with that obtained for the PBS-treated group (data not shown). Collectively, viability of all four breast cancer cell lines were significantly inhibited by the as-synthesized AgNPs ascertaining their anticancer activity toward breast cancer cells (Gurunathan, Han, Eppakayala, Jeyaraj, & Kim, 2013; Gurunathan, Park, Han, & Kim, 2015) on the downright contrast, nonmalignant cells (HEK-293) were comparatively resistant toward NPs at the same concentrations; nevertheless, were susceptible at higher concentration (Figure 3a). The IC_{50} values of the as-synthesized AgNPs were 0.65 and 1.06 μg/ml against MCF-7, 2.95 and 2.83 μg/ml against MDA-MB-231, 2.59 and 3.15 μg/ml against 4T1, and 4.62 and 3.15 μg/ml against LA-7 for BHI-AgNPs and Av-AgNPs, respectively. Thus, both the particles behaved in almost similar fashion for the tested cell line and amongst the various cell line tested, MCF-7 was most sensitive followed by MDA-MB-231, 4T1, and LA-7. Thus, we could instigate that the cytotoxicity of the as-synthesized NPs depends on the cell type under investigation; this is indeed in concordance with previous reports suggesting that besides other underlying issues, cytotoxicity of NPs bears correlation with the cell types examined (AshaRani et al., 2009; Suresh et al., 2012). It is interesting that aggressive and highly metastatic breast cancer cell line (MDA-MB-231 cells) was quite sensitive towards the active NPs (Gurunathan et al., 2013, 2015; Krishnaraj, Muthukumaran, Ramachandran, Balakumaran, & Kalaichelvan, 2014). As a matter of fact, currently, targeted therapy for aggressive breast cancer is very limited; thus the intriguing anticancerous potentials of the as-synthesized AgNPs toward MDA-MB-231 cells merits their candidature for further investigation. Therefore, we selected this in vitro aggressive breast cancer model for our further investigation. Primarily, colony forming assay was used to ascertain dose-dependent inhibition in MDA-MB-231 cells; interestingly, the as-synthesized AgNPs inhibited MDA-MB-231 cells at all the concentration tested (Figure 3b); whereas neither neat BHI nor Av extract exhibited any antiproliferative activities even at the highest concentration (data not shown) which concord well with MTT assay (Figure 3A).

To further assess the mode and magnitude of cell death, phosphatidylserine externalization to the outer leaflet was carried out using annexin V-FITC/PI dual staining using flow cytometry. Following treatment with NPs, there occurred an increase of annexin V-FITC +ve cells (early apoptosis) and annexin V-FITC+ve/PI +ve (late apoptosis) with subsequent decrease in annexin V-FITC-ve/PI-ve (live cells) MDA-MB-231 cells (Figure 4a). In contrast, no changes were observed in PI + ve (necrotic cells) population compared with the untreated control group (Figure 4a). The apoptosis-inducing activity of the as-synthesized AgNPs was further confirmed by evaluating the expression levels of pro- and antiapoptotic cellular protein markers. Intriguingly, there was a significant increment in Bax and Bak expression level; together with a decrement in Bcl-2 and Bcl-xl expression in AgNPs-treated cells compared with untreated control cells (Figure 4b). In addition, cleaved caspase-3 and cleaved PARP level were significantly increased as well following AgNPs treatment (Figure 4b). Collectively, these data suggest that the as-synthesized AgNPs mediated cancer cells death are plausibly due to physiological apoptosis.

Moreover, additional experimentations were performed to further ascertain NPs mediated cellular death. Considering the fact that DNA laddering is a distinctive feature of late apoptosis (Zhang & Xu, 2000); we set about to study DNA fragmentation in MDA-MB-231 cells following treatment with NPs by means of agarose gel electrophoresis. The data clearly support the marked fragmentation of DNA after NPs treatment compared with the untreated control group (Figure 5a). In addition, DNA fragmentation induced by NPs were further validated by quantitative ELISA. Interestingly, there was a significant increment in cellular DNA fragmentation in NPs treated MDA-MB-231 cells compared with neat CM, Av extract, and untreated control ($p < 0.001$; Figure 5b). Cumulatively, these data clearly establish that the NPs effectively induces DNA fragmentation, a signature of an apoptotic event, in MDA-MB-231 cells. All these results further substantiate and corroborate the aforementioned flow cytometric and western blot data (Figure 4).

Moreover, we also examined the effect of NPs on cell cycle; in this regard, basically cell cycle phase distribution was studied by flow cytometry. It was found that following treatment with NPs, there was an accumulation of cells in the S phase, an essential point in cell cycle compared to untreated control cells and more important, increased sub-G1 population was observed following NP treatment which further signifies and substantiates apoptotic cell death (Figure 6). These data clearly suggest that NPs retards the progression of cell cycle and induce hypodiploid nuclei in MDA-MB-231 cells.

As a matter of fact, increased ROS beyond a threshold level drive the cancer cells towards apoptosis. In this regard, prior studies have underscored the role of oxidative stress in the anticancerous potentialities of various NPs including AgNPs; thus to ascertain the role of oxidative stress in NP-induced cancer cell death, MDA-MB-231 cells were stained with oxidant sensing DCFH-DA dye following treatment with NPs (Hamidullah et al., 2015). Interestingly, flow cytometric analysis reveals that there were considerably increased ROS levels in NPs treated MDA-MB-231 cells compared with untreated control cells (Figure 7). These data suggest that NPs induces ROS generation in MDA-MB-231 cells which plausibly drives the cells toward apoptosis.

To further validate the role of ROS in NPs-mediated cytotoxicity; MDA-MB-231 cells were pretreated with NAC (ROS scavenger), incubated with NPs and henceforth cytotoxicity was determined by MTT assay (Guo, Zhang, Huang, Jiang, & Gu, 2015; Hamidullah et al., 2015). Figure 8 shows that AgNPs mediated cell cytotoxicity was significantly inhibited in presence of NAC ($p < 0.05$). As evident, cell viability was considerably reduced upon treatment with BHI-AgNPs

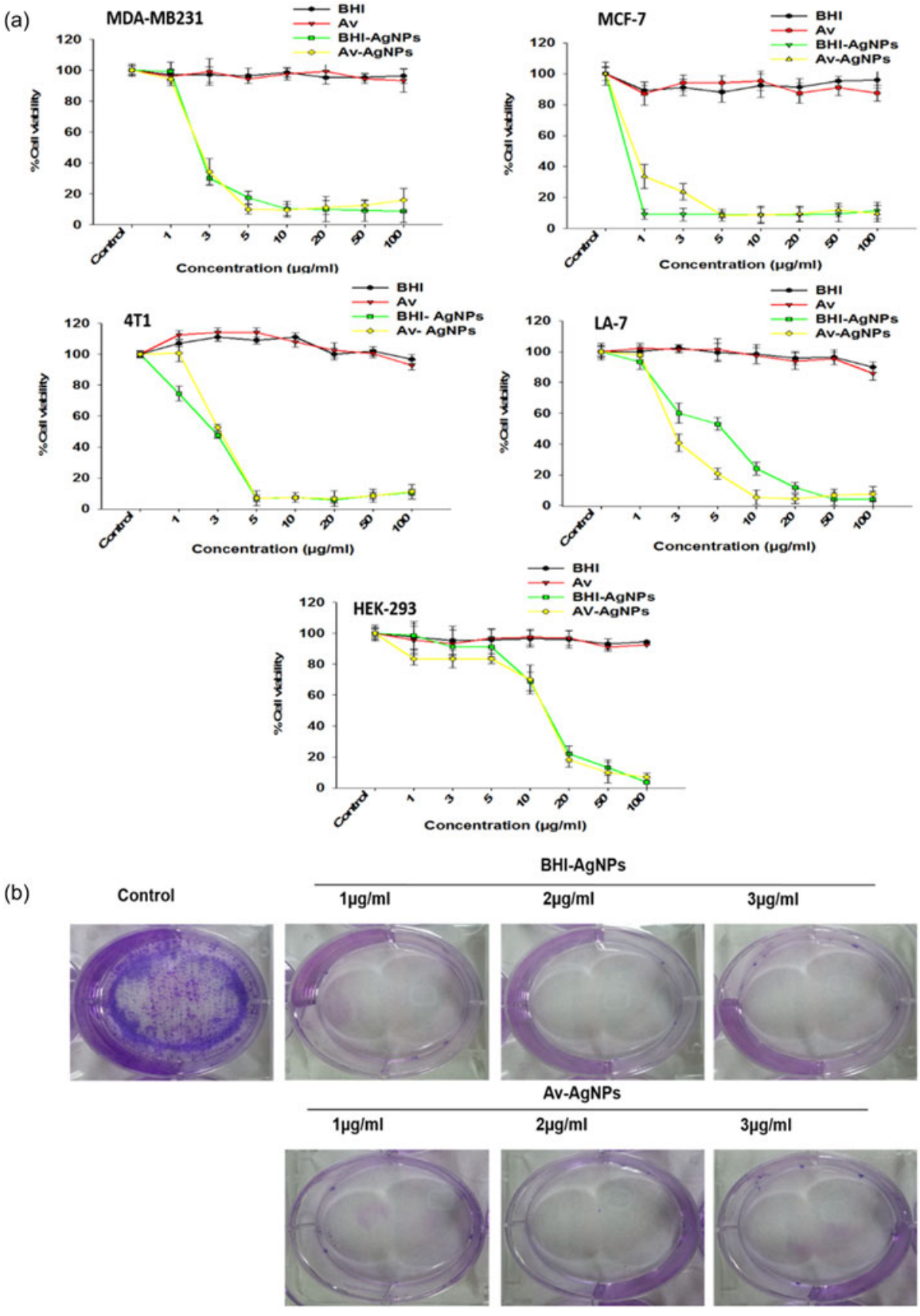

FIGURE 3 Effect of the as-synthesized AgNPs on cell viability of MDA-MB-231, MCF-7, 4T1, LA-7, and HEK-293 cells as determined by MTT assay (a); The effect of as-synthesized AgNPs on colony formation of breast cancer MDA-MB-231cells (b). AgNP: silver nanoparticle; MTT: 3-(4,5-dimethylthiazol-2-yl)-2,5-diphenyltetrazolium bromide [Color figure can be viewed at wileyonlinelibrary.com]

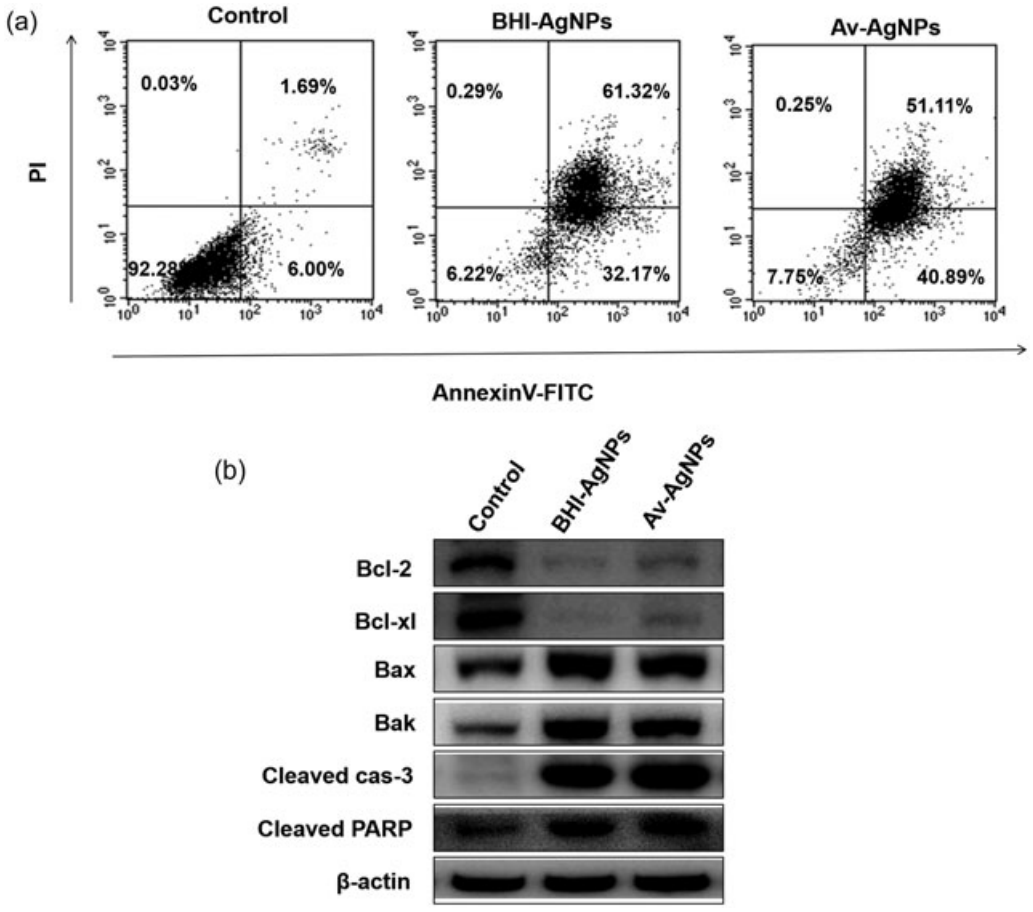

FIGURE 4 Effect of as-synthesized AgNPs on apoptosis in MDA-MB-231 cells. MDA-MB-231 cells were treated with AgNPs, stained with annexin V-FITC/PI and subsequently analyzed by flow cytometry (a); MDA-MB-231 cells were treated with AgNPs and expression of various pro- and antiapoptotic markers were examined by western blot (b). AgNP: silver nanoparticle

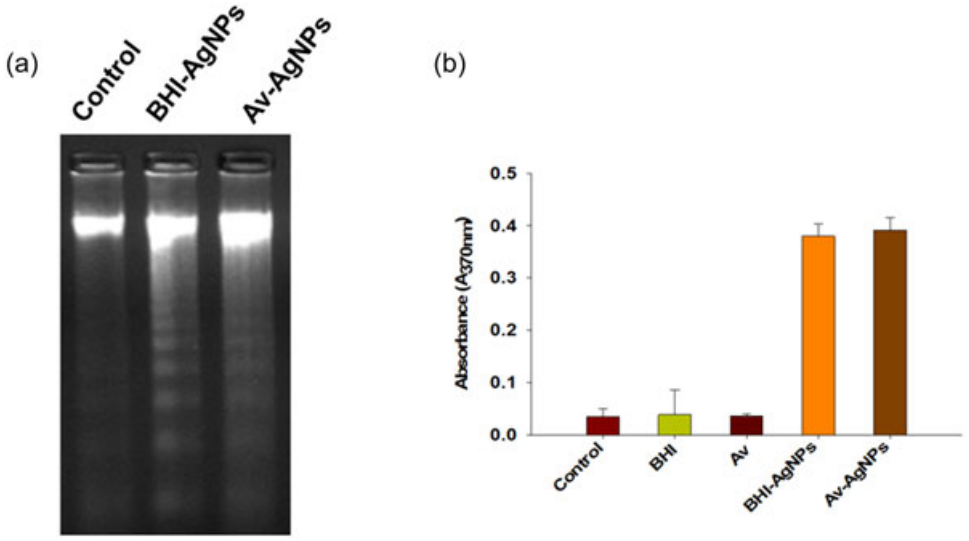

FIGURE 5 Effect of the as-synthesized AgNPs on DNA fragmentation in MDA-MB-231 cells. MDA-MB-231 cells were treated with AgNPs and DNA fragmentation was examined by agarose gel electrophoresis (a) and by BrdU ELISA kit (B). AgNP: silver nanoparticle; BrdU: 5-bromo-2-deoxyuridine [Color figure can be viewed at wileyonlinelibrary.com]

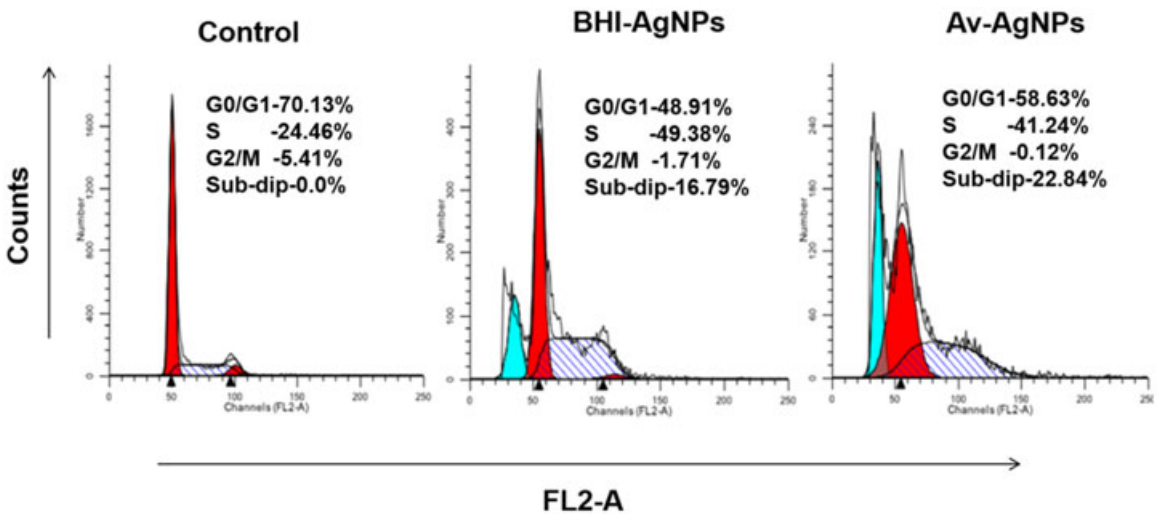

FIGURE 6 Effect of the as-synthesized AgNPs on cell cycle phase distribution in MDA-MB-231 breast cancer cells. MDA-MB-231 cells were treated with as-synthesized AgNPs and cell cycle phase distribution was determined by flow cytometry following staining with PI. AgNP: silver nanoparticle; PI: propidium iodide [Color figure can be viewed at wileyonlinelibrary.com]

and Av-AgNPs respectively. Nevertheless, pretreatment with NAC rescued MDA-MB-231 cells (Figure 8a); thus as the treatment with NAC prevented AgNPs mediated cancer cell death, this clearly suggests ROS dependency in NP induced cancer cell death. In addition, DNA laddering was examined in presence and absence of NAC; interestingly but not surprisingly, it was found that attenuation of ROS by NAC, considerably abrogated NPs mediated DNA fragmentation as clearly evident by DNA fragmentation ELISA (Figure 8b), wherein a significant reduction in absorbance intensity was obtained in the presence of NAC ($p < 0.001$). Concording results were obtained from the DNA ladder assay as well (Figure 8c). Collectively, NAC, a potent antioxidant, significantly abolished AgNPs-mediated cellular responses as evident from MTT assay, DNA ladder assay and quantitative DNA fragmentation ELISA (Figure 8); this plausibly suggests that ROS generation plays a crucial role in NPs mediated cancer cell death.

Lastly, after ascertaining the anticancer potentialities in solitary; we extended further to examine the potentialities of as-synthesized AgNPs in conjunction with ART thereof. Cells were treated with ART together with the different concentrations of the as-synthesized AgNPs, and cell viability was measured in MDA-MB-231, MCF-7, 4T1, and LA-7 cells by MTT assay (Figure 9a). Figure 9a shows that at specific dose of AgNPs (1 μg/ml in case of MDA-MB-231, 4T1, and LA-7 and 0.8 μg/ml in case of MCF-7) no significant reduction in cell viability was observed in any of the breast cancer cell lines; similar observations were obtained for ART as well. Nevertheless, when the cells were treated with ART together with varying concentration of AgNPs, plausible reduction in cell viability was observed in a dose-dependent manner. Intriguingly, cell viability decreased with increasing concentration of AgNPs, and at a maximum concentration of NPs, almost 50% reduction in viability was observed which was statistically

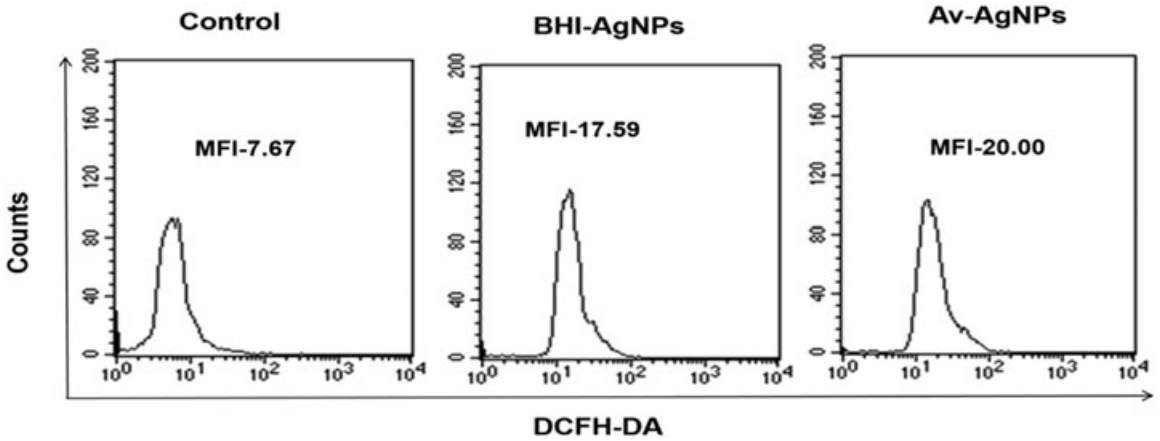

FIGURE 7 Effect of as-synthesized AgNPs on ROS generation in MDA-MB-231 cells. MDA-MB-231 cells were treated with the as-synthesized AgNPs and ROS generation was determined following staining with DCFH-DA using flow cytometry. AgNP: silver nanoparticle; DCFH-DA: 2,7-dichloro dihydro fluorescein diacetate; ROS: reactive oxygen species

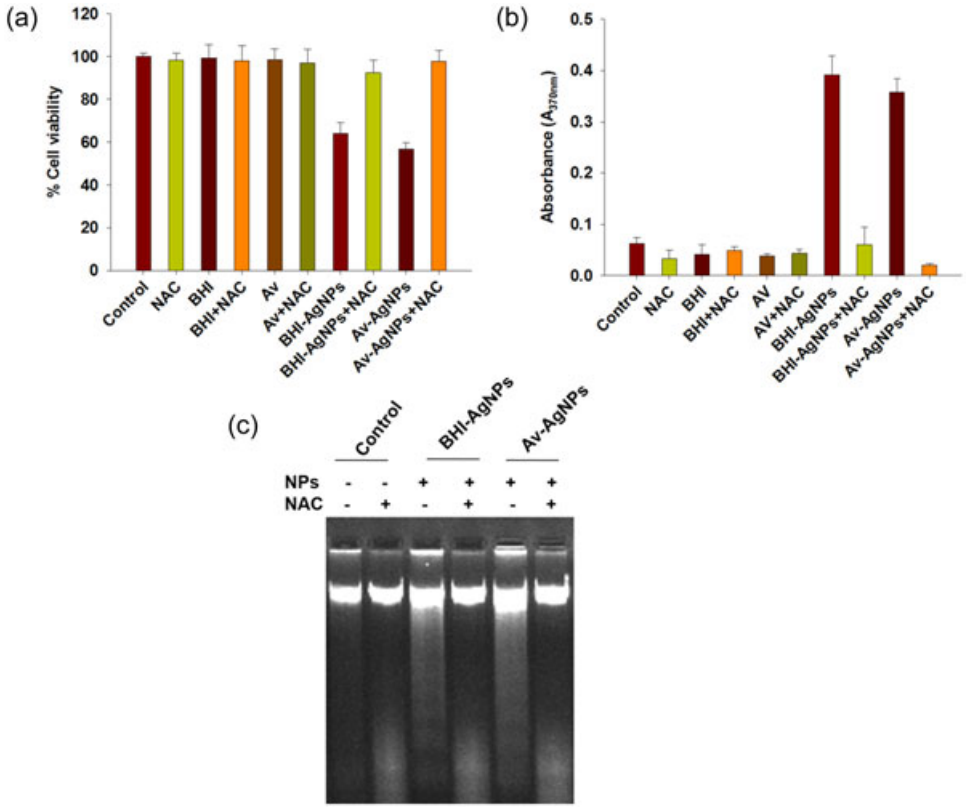

FIGURE 8 Effect of AgNPs-mediated cell cytotoxicity in presence of NAC in MDA-MB-231 cells. MDA-MB-231 cells were pretreated with 10 mM NAC followed by treatment with NPs and cell viability thereof assessed by MTT assay (a); DNA fragmentation was examined in presence of NAC by agarose gel electrophoresis (b); and by BrdU ELISA kit (c). AgNP: silver nanoparticle; BrdU: 5-bromo-2-deoxyuridine; MTT: 3-(4,5-dimethylthiazol-2-yl)-2,5-diphenyltetrazolium bromide; NAC: N-acetyl-L-cysteine; NP: nanoparticle [Color figure can be viewed at wileyonlinelibrary.com]

significant compared with cells treated with either of the entities at the same concentration ($p < 0.05$).

In addition, apoptosis was also evaluated after treatment with ART and AgNPs in MDA-MB-231 cells (Figure 9b). Interestingly, the data suggests that the combinatorial therapy synergistically/efficiently induced apoptosis in MDA-MB-231 breast cancer cells compared with the drugs when given solitarily ($p < 0.05$). Lately, it has been ventured that nanonization of drugs into NPs greatly influences their solubilities, dissolution kinetics, and bioavailability issues besides passively targeting the drugs to tumor sites by exploiting enhanced permeability and retention effects together with the minimization of side effects in the biosystem. It could be speculated that administering ART in combination with AgNPs might have resulted in binding of ART onto the surfaces of the AgNPs which plausibly resulted in the higher intracellular accumulation of the drug (Guo et al., 2015). Albeit, since decades delivery platforms has been in vogue to overcome some of the pharmacological limitations of drugs; unfortunately, as of yet there are few reports on ART-delivery/carrier platforms (Wang et al., 2012). In addition, in these carrier formulated ART, the former merely acts as excipients; and ART is only therapeutically relevant; in this context, the prospective ART-AgNPs amalgam in our ART and AgNPs combinatorial mixture offers attractive benefits as both are therapeutically relevant (Chung et al., 2014); to this end, our specifically formulated ART functionalised AgNPs were exceedingly beneficial with intriguing therapeutic outcomes (unpublished observation). Although the prospective formation of ART-AgNPs is one of the possibility to anticipate for the enhanced efficacy of our ART-AgNPs which concamitantly might have ensued in enhanced binding to cells or augmented uptake by cells. Seemingly there could be other possibilities as well which requires further investigations. Nevertheless, these intricacies plausibly play a role in subduing some of the pharmacological limitations of ART including reduced bioavailability and feeble circulatory half-life.

Besides, it is also equally important to state that this strategy might aid usage of AgNPs at feeble concentration levels henceforth plausibly improves their therapeutic index (Guo et al., 2015). All these issues assist in advancing the therapeutic applicability of the combinatorial amalgam not only against breast cancer but also against other forms of malignant cancer as well. Remarkably, as more and more would be gleaned about their intricacies they could be instrumental in offering better therapeutics against the most deadliest form of diseases.

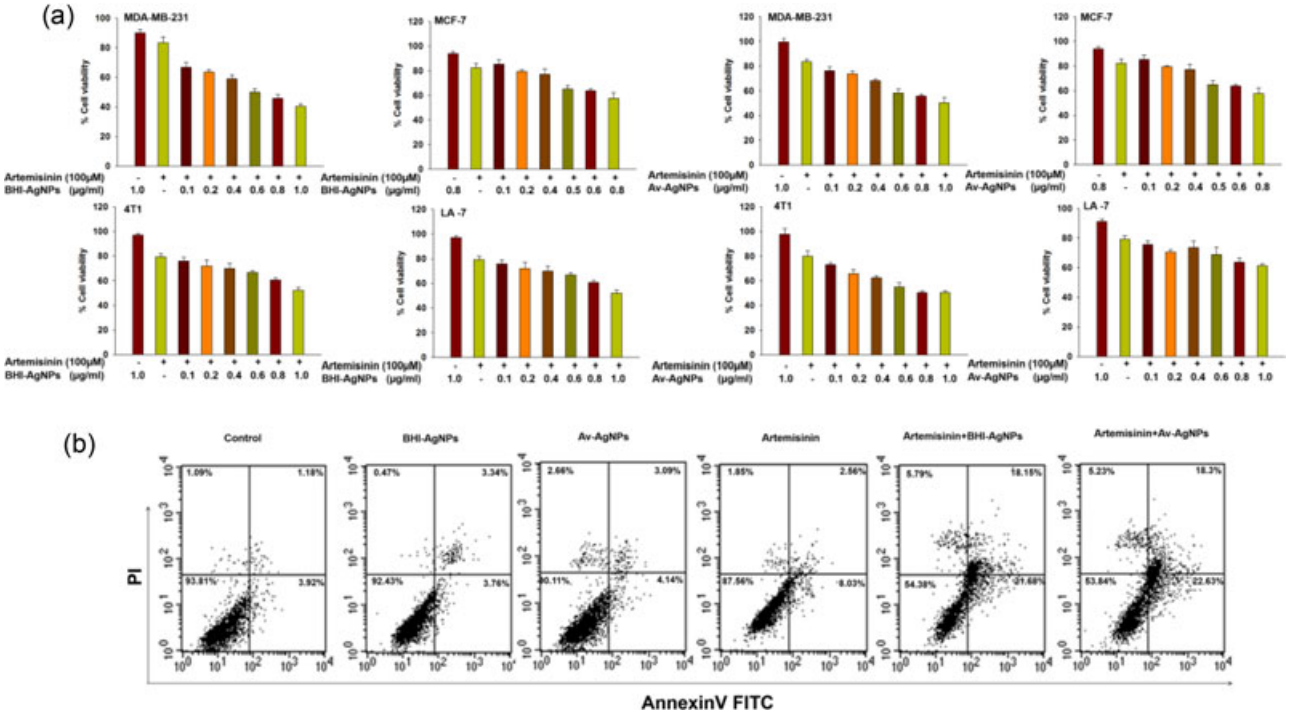

FIGURE 9 (a) Effect of artemisinin-mediated cell cytotoxicity in presence of BHI-AgNPs and Av-AgNPs in MDA-MB-231, MCF-7, 4T1, and LA-7 cells as determined by MTT assay . (b) Effect of artemisinin-mediated apoptosis in presence of BHI-AgNPs and Av-AgNPs in MDA-MB-231 cells as determined by flow cytometry. AgNP: silver nanoparticle; BHI: brain heart infusion; MTT: 3-(4,5-dimethylthiazol-2-yl)-2,5-diphenyltetrazolium bromide [Color figure can be viewed at wileyonlinelibrary.com]

ACKNOWLEDGMENT

Khan Farheen Badrealam and Hamidullah acknowledges the Department of Biotechnology, Govt. of India, for financial support in the form of a senior research fellowship. We are also thankful to Mr. AL Viskwakarma for flow cytometric studies.

CONFLICTS OF INTEREST

The authors report no conflicts of interest in this work.

ORCID

Badrealam Farheen Khan http://orcid.org/0000-0001-9030-4152

REFERENCES

AshaRani, P. V., Low Kah Mun, G., Hande, M. P., & Valiyaveettil, S. (2009). Cytotoxicity and genotoxicity of silver nanoparticles in human cells. *ACS Nano*, *3*(2), 279–290.

Chandran, S. P., Chaudhary, M., Pasricha, R., Ahmad, A., & Sastry, M. (2006). Synthesis of gold nanotriangles and silver nanoparticles using *Aloe vera* plant extract. *Biotechnology Progress*, *22*(2), 577–583.

Chung, J. E., Tan, S., Gao, S. J., Yongvongsoontorn, N., Kim, S. H., Lee, J. H., … Ying, J. Y. (2014). Self-assembled micellar nanocomplexes comprising green tea catechin derivatives and protein drugs for cancer therapy. *Nature Nanotechnology*, *9*(11), 907–912.

Crespo-Ortiz, M. P., & Wei, M. Q. (2012). Antitumor activity of artemisinin and its derivatives: From a well-known antimalarial agent to a potential anticancer drug. *Journal of Biomedicine & Biotechnology*, *2012*, 247597.

Guo, D., Zhang, J., Huang, Z., Jiang, S., & Gu, N. (2015). Colloidal silver nanoparticles improve anti-leukemic drug efficacy via amplification of oxidative stress. *Colloids and Surfaces, B: Biointerfaces*, *126*, 198–203.

Gurunathan, S., Park, J. H., Han, J. W., & Kim, J. H. (2015). Comparative assessment of the apoptotic potential of silver nanoparticles synthesized by *Bacillus tequilensis* and *Calocybe indica* in MDA-MB-231 human breast cancer cells: Targeting p53 for anticancer therapy. *International Journal of Nanomedicine*, *10*, 4203–4222.

Gurunathan, S., Han, J. W., Eppakayala, V., Jeyaraj, M., & Kim, J. H. (2013). Cytotoxicity of biologically synthesized silver nanoparticles in MDA-MB-231 human breast cancer cells. *BioMed Research International*, *2013*, 535796.

Gurunathan, S., Kalishwaralal, K., Vaidyanathan, R., Venkataraman, D., Pandian, S. R. K., Muniyandi, J., … Eom, S. H. (2009). Biosynthesis, purification and characterization of silver nanoparticles using *Escherichia coli*. *Colloids and Surfaces, B: Biointerfaces*, *74*(1), 328–335.

Hamidullah, Saini, K. S., Ajay, A., Devender, N., Bhattacharjee, A., Das, S., … Konwar, R. (2015). Triazole analog 1-(1-benzyl-5-(4-chlorophenyl)-1H-1,2,3-triazol-4-yl)-2-(4-bromophenylamino)-1-(4 -chlorophenyl) ethanol induces reactive oxygen species and autophagy-dependent apoptosis in both in vitro and in vivo breast cancer models. *The International Journal of Biochemistry & Cell Biology*, *65*, 275–287.

Jo, J. H., Singh, P., Kim, Y. J., Wang, C., Mathiyalagan, R., Jin, C. G., & Yang, D. C. (2016). Pseudomonas deceptionensis DC5-mediated synthesis of extracellular silver nanoparticles. *Artificial Cells Nanomedicine, and Biotechnology*, *44*(6), 1576–1581.

Key, T. J., Verkasalo, P. K., & Banks, E. (2001). Epidemiology of breast cancer. *The Lancet Oncology*, *2*(3), 133–140.

Krishna, S., Bustamante, L., Haynes, R. K., & Staines, H. M. (2008). Artemisinins: Their growing importance in medicine. *Trends in Pharmacological Sciences*, *29*(10), 520–527.

Krishnaraj, C., Muthukumaran, P., Ramachandran, R., Balakumaran, M. D., & Kalaichelvan, P. T. (2014). *Acalypha indica* Linn: Biogenic synthesis of silver and gold nanoparticles and their cytotoxic effects against MDA-MB-231, human breast cancer cells. *Biotechnology Reports*, *4*, 42–49.

Kumar, C. G., & Poornachandra, Y. (2015). Biodirected synthesis of Miconazole-conjugated bacterial silver nanoparticles and their application as antifungal agents and drug delivery vehicles. *Colloids and Surfaces, B: Biointerfaces*, *125*, 110–119.

Oves, M., Khan, M. S., Zaidi, A., Ahmed, A. S., Ahmed, F., Ahmad, E., … Azam, A. (2013). Antibacterial and cytotoxic efficacy of extracellular silver nanoparticles biofabricated from chromium reducing novel OS4 strain of *Stenotrophomonas maltophilia*. *PLoS One*, *8*(3), e59140.

Senapati, S., Ahmad, A., Khan, M. I., Sastry, M., & Kumar, R. (2005). Extracellular biosynthesis of bimetallic Au-Ag alloy nanoparticles. *Small*, *1*, 517–520.

Shankar, S. S., Rai, A., Ankamwar, B., Singh, A., Ahmad, A., & Sastry, M. (2004). Biological synthesis of triangular gold nanoprisms. *Nature Materials*, *3*(7), 482–488.

Shivaji, S., Madhu, S., Singh, S. (2011). Extracellular synthesis of antibacterial silver nanoparticles using psychrophilic bacteria. *Process Biochemistry*, *46*, 1800–1807.

Singh, P., Kim, Y. J., Singh, H., Wang, C., Hwang, K. H., Farh, M., & Yang, D. C. (2015). Biosynthesis, characterization, and antimicrobial applications of silver nanoparticles. *International Journal of Nanomedicine*, *10*, 2567–2577.

Suresh, A. K., Pelletier, D. A., Wang, W., Morrell-Falvey, J. L., Gu, B., & Doktycz, M. J. (2012). Cytotoxicity induced by engineered silver nanocrystallites is dependent on surface coatings and cell types. *Langmuir*, *28*(5), 2727–2735.

Wang, Z., Yu, Y., Ma, J., Zhang, H., Zhang, H., Wang, X., … Zhang, Q. (2012). LyP-1 modification to enhance delivery of artemisinin or fluorescent probe loaded polymeric micelles to highly metastatic tumor and its lymphatics. *Molecular Pharmaceutics*, *9*(9), 2646–2657.

Wei, L., Lu, J., Xu, H., Patel, A., Chen, Z. S., & Chen, G. (2015). Silver nanoparticles: Synthesis, properties, and therapeutic applications. *Drug Discovery Today*, *20*(5), 595–601.

Xie, J., Lee, J. Y., Wang, D. I. C., & Ting, Y. P. (2007). Silver nanoplates: From biological to biomimetic synthesis. *ACS Nano*, *1*(5), 429–439.

Xu, Q., Li, Z., Peng, H., Sun, Z., Cheng, R., Ye, Z., & Li, W. (2011). Artesunate inhibits growth and induces apoptosis in human osteosarcoma HOS cell line in vitro and in vivo. *Journal of Zhejiang University. Science. B*, *12*(4), 247–255.

Yamal, G., Sharmila, P., Rao, K. S., & Pardha-Saradhi, P. (2013). Inbuilt potential of YEM medium and its constituents to generate Ag/Ag(2)O nanoparticles. *PLoS One*, *8*(4), e61750.

Zhang, J. H., & Xu, M. (2000). DNA fragmentation in apoptosis. *Cell Research*, *10*(3), 205–211.

SUPPORTING INFORMATION

Additional supporting information may be found online in the Supporting Information section at the end of the article.

How to cite this article: Khan BF, Hamidullah, Dwivedi S, Konwar R, Zubair S, and Owais M. Potential of bacterial culture media in biofabrication of metal nanoparticles and the therapeutic potential of the as-synthesized nanoparticles in conjunction with artemisinin against MDA-MB-231 breast cancer cells. *J Cell Physiol*. 2018;1–14. https://doi.org/10.1002/jcp.27438